Technology Milestone Report

EXCEDE Technology Milestone #1: Monochromatic Contrast Demonstration Completion Report

Glenn Schneider[1] (PI), Ruslan Belikov[2], Sandrine Thomas[2], Eugene Pluzhnik[2], Julien Lozi[1], Paul Davis[2], Dana Lynch[2], Thomas Greene[2], Olivier Guyon[1], Eric Smith[3]

[1] The University of Arizona, [2] NASA/Ames Research Center, [3] Lockheed Martin

December 02, 2013

Approvals:

Released by

[signature: Glenn Schneider]

Glenn Schneider
Principal Investigator

02 Dec 2013
Date

Approved by

[signature: Peter Lawson]
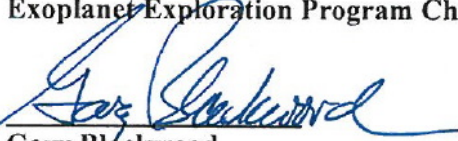
Peter Lawson
Exoplanet Exploration Program Chief Technologist, JPL

2/12/14
Date

[signature: Gary Blackwood]
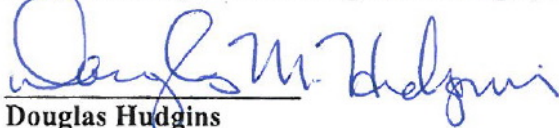
Gary Blackwood
Exoplanet Exploration Program Manager, JPL

2/13/14
Date

[signature: Douglas Hudgins]
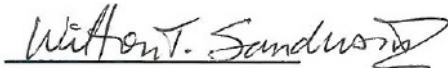
Douglas Hudgins
Exoplanet Exploration Program Scientist, NASA HQ

2/19/2014
Date

[signature: Wilton T. Sanders]

Wilton Sanders
Explorer Program Scientist, NASA HQ

2/19/2014
Date

[signature: John Gagosian]

John Gagosian
Exoplanet Exploration Program Executive, NASA HQ

2/19/2014
Date

Table of Contents

1. Preamble

This EXCEDE Milestone #1 Closure Report (this document) is predicated upon the Technology Maturation & Demonstration (TM&D) goals as set forth in the "EXCEDE Technology Milestone #1: Monochromatic Contrast Demonstration" test plan (JPL Document D-75789). The latter document, as a primary reference, should be consulted to gain a background understanding of: (a) the overall objectives of the EXCEDE TM&D program including traceability to science objective and mission goals, (b) an introduction to Phase Induced Amplitude Apodization (PIAA) coronagraphy and its applicability with wavefront error sensing and control to the EXCEDE measurement and instrument requirements, (c) a description of the TM&D plan, (d) definitions and computations of performance metrics, and (e) criteria for evaluating success, which are not replicated in this report.

The laboratory TM&D program for EXCEDE Milestone #1 was conducted using facilities of the NASA/Ames Research Center's (ARC) Coronagraph Experiment Laboratory under the programmatic direction of Glenn Schneider (PI, UofA) and technical leadership of Ruslan Belikov (NASA/ARC). The laboratory TM&D program for Milestone #1 was carried out from April 2012 – September 2013. TM&D milestone #1, as expressed in JPL Document D-75789 (and see § 2 of this document), was fully realized as a result of this phase of the EXCEDE technology development program.

2. Introduction -- Milestone #1

This report describes the laboratory completion of the EXCEDE TM&D milestone #1, as defined in JPL Document D-75789 to:

"Demonstrate using Phase-Induced Amplitude Apodization a raw contrast median level 10^{-6} between a 1.2 λ/D inner working angle and 2 λ/D, simultaneously with a median level of 10^{-7} between 2 λ/D and 4 λ/D, in monochromatic light at any single wavelength in the range of 400 nm ≤ λ ≤ 900 nm over a single-sided dark zone."

The milestone objective was pursued, and successfully completed, using an in-air laboratory test bed at the NASA Ames Coronagaph Experiment (ACE) facility as described in § 3 of this document.

This milestone was formulated in support of the Exoplanetary Circumstellar Environments and Disk Explorer (EXCEDE) [1], an EX-class EXPLORER mission proposed to NASA under the ROSES 2010 (EXPLORER 2011) mission Announcement of Opportunity and selected by NASA for TM&D as a Category III investigation. The EXCEDE mission and instrument concept uses a 0.7-m diameter off-axis telescope to perform high contrast imaging of the circumstellar environments of nearby stars to study the formation, evolution, architectures, and diversity of exoplanetary systems, and characterize circumstellar environments into stellar habitable zones. The EXCEDE technology development program is focused on its starlight suppression system, and includes two TM&D benchmarks to be achieved through laboratory experimentation:

(1) reaching 10^{-6} raw contrast between 1.2 and 2 λ/D in monochromatic light, *simultaneously* with 10^{-7} raw contrast between 2 and 4 λ/D (Milestone #1). This milestone addresses

narrow spectral bandwidth starlight suppression at a small inner working angle, as implemented with a combination of PIAA coronagraphy (a high-efficiency pupil-remapping technique enabling high-contrast imaging at a small inner working angle; 1.2 λ/D for the configuration to be tested) and wavefront error sensing and control [2-11].

(2) replicating Milestone #1 contrast performance in broadband light (10% spectral bandwidth). This is Milestone #2 as spoken to in JPL Document D-75789.

The report describes the completion of Milestone #1.

Technology Milestones serve to gauge the developmental progress of technologies required for space-based missions. In the case of EXCEDE, the ability to perform high contrast imaging observations of exoplanetary debris systems, in conformance with instrumental performance requirements to meet the science mission objectives, are demonstrated through the attainment of TD&M milestones #1 and #2. Successful attainment of technology milestones inform on the mission's readiness to proceed from pre-Phase A to Phase A and beyond.

The completion of a technology milestone is documented through a closure report by the Principal Investigator for review by NASA HQ. This report provides: (1) the information necessary to understand the conditions under which EXCEDE milestone #1 was achieved, (2) a description of the laboratory experiment, tests and demonstrations performed, and (3) a description of the data obtained and the results derived sufficient to certify the attainment of the milestone.

3. Description of Laboratory Configuration

3.1. Overview

The milestone #1 results, reported in § 4, were achieved using the ACE in-air test bed facility that is capable of controlling/suppressing thermal and air-turbulence disturbances to a level required for the EXCEDE TD&M experiments. In addition to the PIAA coronagraphic optics, key components undergoing test were operated as an integrated system to reach the requisite image contrasts. This includes both a deformable mirror using precise calibration, and wavefront error control algorithms, and a low-order wavefront sensor. Two wavefront control algorithms were used to create the "dark zone" and to establish the level of simulated starlight suppression of the integrated system: Electric Field Conjugation (EFC) [17] and Speckle Nulling (SN) [18].

The ACE test bed (Figure 1) is designed for flexible and rapid testing of coronagraph technologies prior to full performance verification in vacuum. ACE began operations in March 2008, and provides a thermally-stabilized in-air, as opposed to vacuum, environment. For experiments not requiring a vacuum environment to reach the same levels of environmental stability, ACE beneficially makes accessing and reconfiguring the experimental layout easier and cheaper. The ACE in-air test bed complements vacuum facilities, such as the test chamber being used by the EXCEDE project at the Lockheed Martin Advanced Technology Center (Palo Alto)

for further technology readiness advancement and the JPL High Contrast Imaging Test bed that has been used for complementary PIAA experimentation at larger IWAs.

Figure 1: Actively stabilized thermal enclosure of the NASA Ames Coronagraph test bed.

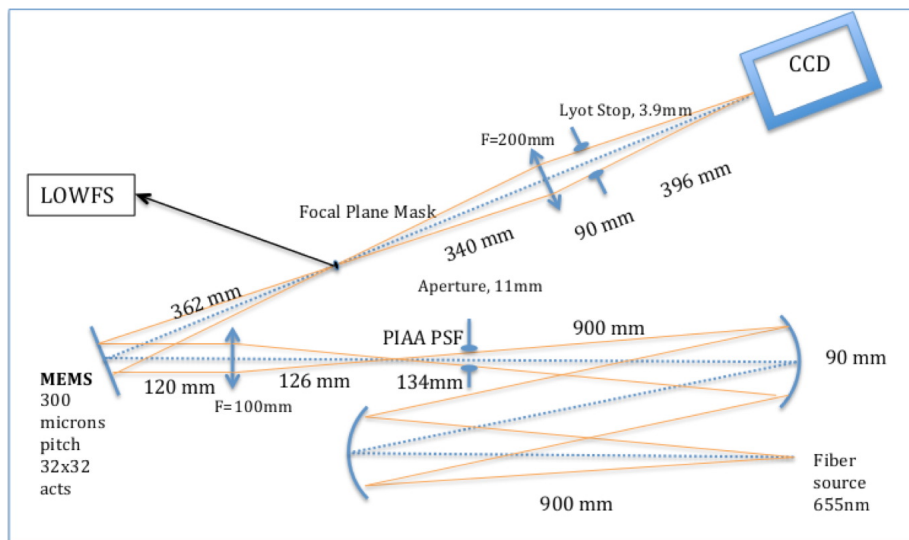## 3.2. Optical Configuration

Figure 2: ACE test bed layout.

The primary components of the optical design and experimental system key to the Milestone #1 demonstration are the PIAA coronagraphic optics to losslessly remap the pupil while eliminating diffraction rings, a 1024 (32x32) actuator MicroElectro Mechanical System Deformable Mirror (MEMS DM) from Boston Micromachines Corporation to control the

6

wavefront errors and, a Low Order Wavefront Sensor (LOWFS) in closed-loop to mitigate low order, time-variable, aberrations ("tip/tilt" errors). We schematically depict the optical layout, showing the placement of the key optical components on the test bed, in Figure 2.

Simulated starlight from a monochromatic laser source is injected in the system using an optical fiber connected to an XYZ-translation stage. The stage is motorized and in closed-loop control with the LOWFS. The light then goes directly to a set of two identical PIAA mirrors, made by Tinsley. Their active diameters are 90 mm and their equivalent focal lengths are 900 mm. However, the clear aperture (pupil image size) was 87.77 mm and slightly underfilled PIAA mirror M1, which is subsequently remapped to a beam spot of size 73.9 mm at PIAA mirror M2. This was done to mitigate several effects that are difficult to control and model on the edges of the beam: errors on the edges of PIAA M1 and the DM are higher than the rest of the mirror, and diffraction effects change the edges of the beam more than the middle.

The magnification of the on-axis beam is x3.5, meaning that the marginal rays are mostly concentrated on a diameter 3.5 times smaller at the output of the PIAA system than at the input. An aperture stop (designated PIAA PSF in Fig 2), slightly smaller than the beam size, is then used to remove wavefront errors introduced by the edges of the PIAA mirrors. The MEMS DM is placed after a re-imaging lens in a converging beam before the focal plane mask. The focal plane mask is selectable on a translation stage as either a circular, or C-shaped, occulter with identical central, reflective, dots in the center of each, on a piece of glass. In both cases[1], the dot is reflective and sends the central light (the low order modes) to the LOWFS. The LOWFS filters fast tip/tilt motions by sending corrections to the input fiber with a cutoff frequency of 10 Hz. (In a flight instrument architecture, the LOWFS closed loop with the input fiber would be replaced with a fast steering mirror). It also measures and corrects for pointing shifts introduced in the system originating from instabilities or wavefront control algorithms. More details on the LOWFS can be found in [10].

A Lyot stop is placed in the converging beam produced by a final re-imaging lens. It is conjugated neither to the MEMS DM, nor to the first PIAA mirror, mainly due to opto-mechanical constraints; On the test bench layout, an iris used as the Lyot mask could not close to the proper size if placed in the plane conjugated to the MEMS DM. This, however, is not crucial to this experiment because the current set up does not have (and does not need) a set of inverse PIAA mirrors. Therefore, the position of the pupil is not as well defined and precise as if calculated using standard geometrical optics. The other consequence of not having an inverse PIAA, is that the final point spread function (PSF), called PSF_{sky}, is more magnified than the PSF found without the PIAA (called PSF_{system}). The magnification, PSF_{sky} / PSF_{system} is 3.5 (equal to the magnification of the on-axis beam in the PIAA system).

N.B.: In compliance with the wavelength requirement for the Milestone #1 demonstration, a 655 nm laser was used as the input source. This fiber-fed source provided the "starlight" signal for all aspects of the demonstration.

---

[1] While both masks were available to use, in our experimentation leading to the demonstration of milestone #1, the circular occulting mask was employed.

The test bed hardware is primarily controlled using Labview, a commercial S/W product using custom modules developed by the experiment team. These modules includes the position control of the optical fiber, the mask position, the deformable mirror, and the LOWFS and science camera.

3.3. Wavefront Control Algorithms

Because of aberrations and residual diffraction, using a coronagraph alone is insufficient to achieve the EXCEDE contrast requirements. One also needs to use wavefront control, or "nulling", techniques to create darker stellocentric regions. Nulling techniques have been demonstrated in multiple independent laboratories, as well as with instruments such as GPI [19], P1640 [20] and SCExAO [21-22] in different contrast and IWA domains. The two techniques used at the ACE laboratory are the Electric Field Conjugation (EFC) [17] and speckle nulling [18] (SN) algorithms. EFC is fast and has the ability to measure the incoherent light in the system, but is dependent upon the fidelity of the optical model of the system. On the other hand, SN, even though slower, is more robust.

Both algorithms allow us to reach the EXCEDE raw contrast requirements from 1.1 to 3.6 λ/D. However, the region from 3.7 to 4 λ/D (on the sky) falls close to the outer range of the MEMS DM's control area in the test configuration and the EFC algorithm is unable to fully reconstruct the wavefront and therefore struggles to create the proper dark zone. Potential explanations include algorithm shifts of the PSF photocenter as well sampling errors in the model. Deficiencies in model fidelity can also arise from non-identified discrepancies between the model and the actual test bed layout. Additionally our model of the MEMS DM does not reproduce its behavior in the high spatial frequency domain as well as it does at low spatial frequencies. These are still on-going areas of research, but do *not* limit our capability to reach contrast performance levels required for Milestone #1.

Both wavefront control algorithms displace the PSF photocenter by asymmetrically shifting the PSF halo (but not the core) as shown in Figure 3. The PSF core remains stationary. In our definition of contrast, we are using the PSF photocenter as the location of the star. In order to keep the PSF centered we used the LOWFS, which determines the location of the PSF photocenter and stabilizes its position as the wavefront error control algorithm is running.

These PSF shifts do *not* affect our Inner Working Angle (IWA) measurement, which is always a relative measurement. Only the exact boundaries of the dark zone – a small fraction of λ/D – will be affected.
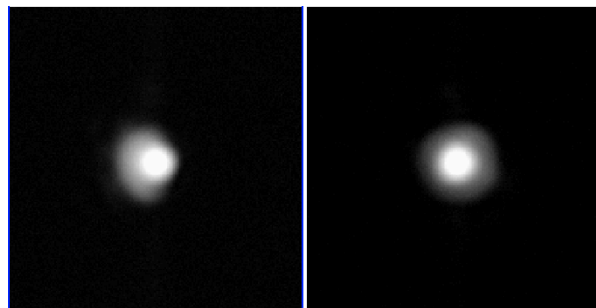

Figure 3: Drift in the PSF before (left) and after (right) LOWFS correction

3.4. System Calibrations

A) Initial calibration (one time calibration)

1- Determination of the Image Scale of the Detector (λ/D per pixel)

We use the science camera detector to measure the image contrast at the detector focal plane (in addition to using it to sense mid-spatial frequency errors in the wavefront error control loop without non-common path errors). Thus, the image scale, P, at the science camera detector focal plane in units of detector pixels per λ/D, must be known in order to calibrate the image contrast as a function of stellocentric angular distance in the same units. We do this (to cross-check the calibration) by two methods: (1) DM Modulation, and (2) Fiber Tip Translation.

Method 1 - DM Modulation: We modulate the surface of the DM with a sine-wave of a given spatial frequency[2], ν_{dm} (e.g., as visualized in Fig 4). The surface of the DM then acts as a reflective diffraction grating producing a reseau pattern of induced "speckles" at the final focal plane imaged by the science camera (see section 3.4.C). In a system *without* upstream PIAA optics, and with optical surfaces only normal to the optical axis, the spatial scale of the reseau peaks as seen on the detector, as a function of the DM modulation, is calculable as:

$P_{sys}(\lambda/D) = L/2/\nu_{dm}*P_{act}*N_{act}/D_{dm}$, [EQ 1]

where: L is the distance between the sine-wave diffraction spots on the detector in pixels

ν_{dm} is the spatial frequency of the sine-wave

P_{act} is the actuator spacing (300 μm)

N_{act} is the number of actuators per axis on the DM (32).

D_{dm} is the diameter of the pupil image on the DM (8 mm),

from which we find $P_{sys}(\lambda/D) = 5.8$ pixels per λ/D at the detector focal plane.

In our test bed configuration, however, the surface of the DM is tilted w.r.t. a surface perpendicular to the optical axis[3] (see, schematically, Fig 3), with the tilt in the direction of the "y" axis of the DM actuator matrix. This results in $P_{sys}(\lambda/D)$ having different scales in the orthogonal "x" and "y" dimensions, such that in our test bench:

$P_{sys}(\lambda/D)_{x,y} = (5.82, 5.88)_{x,y}$ pixels per λ/D.

Using the forward PIAA optics only (i.e., no inverse PIAA mirror system, as none is needed for this experiment) produces a magnification with a scale factor S. To determine S we use a simulation of off-axis point sources passing through PIAA and measure the displacement of the PSF centroid after PIAA relative to the displacement of the original point source (see off_axis_PIAA2.m, provided with the Certification Data Package). From this we find an approximate magnification scale factor with the forward (only) PIAA optics is $S \approx 3.4$. Thus, the test bench image scale at the science camera detector, with the PIAA optics by this method is:

---

[2] In practice, we injected surface patterns into the DM with sinusoidal spatial frequencies over a range from 8 to 1 cycles per aperture, to cross-check measurement results.

[3] The difference in $P_{sys}(\lambda/D)_x$ and $P_{sys}(\lambda/D)_y$ with the tilted DM in the test bed configuration arises from the fact that the projection of the 11mm pupil on the DM is not symmetric, and so the number of actuators illuminated in orthogonal directions across the DM surface will be different.

$P_1(\lambda/D)_{x,y} \approx (19.8, 20.0)_{x,y}$ pixels[4] per λ/D.

The above, however, does not account for the fiber illumination on the PIAA M1 mirror in the test bed setup that was found to be decreased by 54% at the edge of the subaperture. After correcting for this effect, S' = 3.52, and thus:

$P_{1\_PIAA}(\lambda/D)_{x,y} = (20.5, 20.7)_{x,y}$ pixels per λ/D, specifically for the as-implemented test bed[4].

Method 2 – Fiber Tip Translation: The image scale derived above was independently determined by a more direct (and likely more accurate) method that relies on measuring the distance between the optical elements. This is done by laterally displacing the input fiber by known controlled amounts and measuring the resulting displacement of the image centroid recorded on the science camera (with its detector at the final focal plane). The ratio between the two was determined to be $F_{x,y} = (0.357 \pm 0.003, 0.356 \pm 0.003)_{x,y}$ microns per pixel. We then calculated the conversion between off-axis sky angle (in units of λ/D) and the point source lateral displacement in microns[5].

$P_{2\_PIAA}(\lambda/D)_{x,y} = (18.87, 18.86)_{x,y}$ pixels per λ/D.

We used this calibration to position the mask at 1.2 λ/D. The only measurement errors come from establishing the relationship of the displacement of the fiber in microns and camera pixels, and in measuring the PSF image centroid positions. When combined in quadrature, the 1-σ per axis uncertainty is $\sim \pm 0.2$ pixels per λ/D, a more accurate ($\pm \sim 1\%$) result than with Method 1. Since $P_{1\_PIAA}(\lambda/D)_{x,y}$ and $P_{2\_PIAA}(\lambda/D)_{x,y}$ are in statistical agreement, we adopt $P_{2\_PIAA}(\lambda/D)_{x,y}$ given its intrinsically smaller optical model-independent uncertainties (though $P_{1\_PIAA}(\lambda/D)_{x,y}$, as an independent expectation value, serves as a useful cross-check).
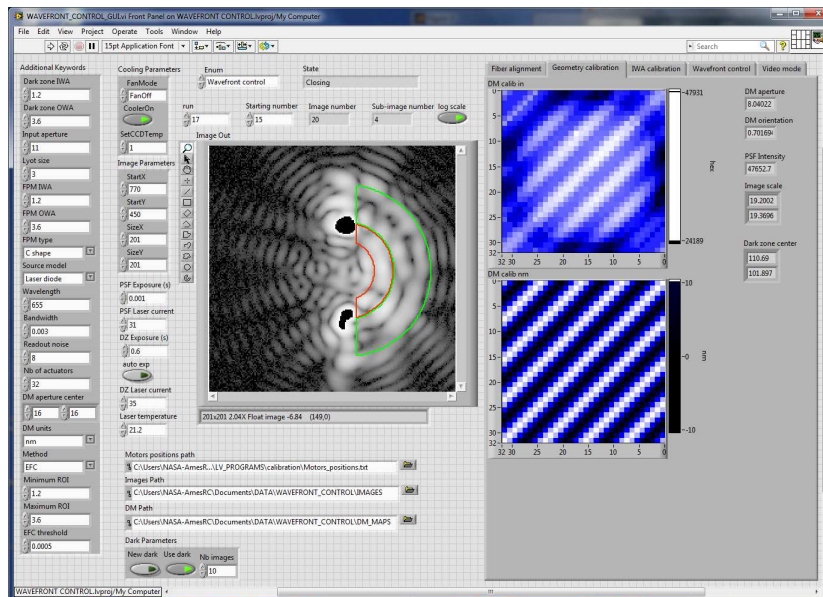

Figure 4 : System Calibration GUI display of sine-waves modulation pattern on the DM (right panels).

---

[4] The uncertainties in the exact metrology of the optical elements in the test bed system lead to a total uncertainty in this determination of $P_{sys}(\lambda/D)_{x,y}$ of $\pm$ approximately 5%.

[5] As codified in the module Calculate_fiber_scale.m, delivered as part of the CDP.

2 - *Deformable Mirror Characterization*

The EFC algorithm and to a lesser extent, SN[6], rely on the following DM characterizations: the DM deflection curves (displacement of an actuator to a given applied voltage); the influence function; and a "flat" voltage map which produces a flat DM surface (with all voltages at 0, the DM has some non-flatness dominated by defocus and astigmatism modes). The deflection curves were measured for all actuators and influence functions were measured for some actuators. The variations of deflection curves and influence functions between different actuators were very small and a representative deflection curve and influence function was adopted for all actuators in our models for simplicity. All three characterizations where performed by Norton and Thomas in 2009 at the Laboratory for Adaptive Optics at the University of California Santa Cruz.

This characterization was adopted, and verified (but not re-derived), on the EXCEDE test bed in the ACE laboratory, by commanding the DM flat (and also imprinting other surface influence functions) prior to starting the EXCEDE Milestone #1 demonstrations.

3 - *Pupil Illumination Calibration*

EFC also requires knowledge of the intensity profile illuminating the DM. The intensity was measured directly by reimaging the DM onto the science camera by inserting a reimaging lens. The comparison to models yielded an excellent match in the bright portion of the beam, and an adequate match on the edges (where the illumination is weak), 'excellent' in the sense that EFC delivers the milestone performance.

B) Trial Run Calibrations (every run)

The EXCEDE Milestone #1 stellocentric raw median image contrast requirements as a function of stellocentric angle require both an accurate calibration of the test bed hardware and maintaining that calibration over time (system stability). Of key importance are the calibrations of: (1) the optical alignment (metrology) of the fiber that feeds the system with simulated starlight, (2) the image (Fresnel diffraction) scale at the science camera focal plane and as it propagates through the optical system, (3) the intensity of the simulated starlight, and the temporal stability of all three. The calibrations of these system elements have been codified in an executable Labview module with a graphical user interface (GUI; see Fig 4 – 6) for flexibility, ease of operation, and real-time execution feedback, called Wavefront_Control_GUI.lv that is provided as part of the CDP. These calibrations are re-established with each trial run of the test bench starlight suppression system.

---

[6] EFC is implemented in MATLAB. SN is implemented in C and communicates the requisite actuator strokes in raw (12 bit) ADUs, whereas the EFC algorithm interface is in units of microns, with the a priori determined calibration between voltage, stroke, and ADUs implemented in the S/W module EFC_Hex2nm.m, provided in the CDP. Some details of that calibration and device operation: The maximum voltage is +216 volts. The scaled conversion between ADUs and DM voltages is DMvoltages_volts = 216 * sqrt(DMVoltages_hex). The calibration from voltages to nanometers as found by Norton & Thomas 2009 as adopted is: DMnm = -0.32446 * DMVoltages_volts + 0.04085 * DMVoltages_volts ^2. (As an interface detail, the array format convention between the EFC algorithm and the Labview code are transposed).

1 - Fiber alignment

The input optical fiber is aligned to the PIAA optics. The fiber head is mounted on two independently commanded stages: one with electric motors (long range travel but slow and with hysteresis), and one with piezo-electric actuators (small range travel, but fast). The electric motors enable the alignment of the fiber with respect to the PIAA mirrors. During this alignment process, the piezos are left at their mid-range of travel, and electric motor position is tuned to maximize the sharpness[7] of the PSF. The piezos are used in the LOWFS sensing and control loop to compensate for tip/tilt misalignments. Figure 5 (right panels) illustrates the result of a fiber tip calibration, as presented by the GUI.
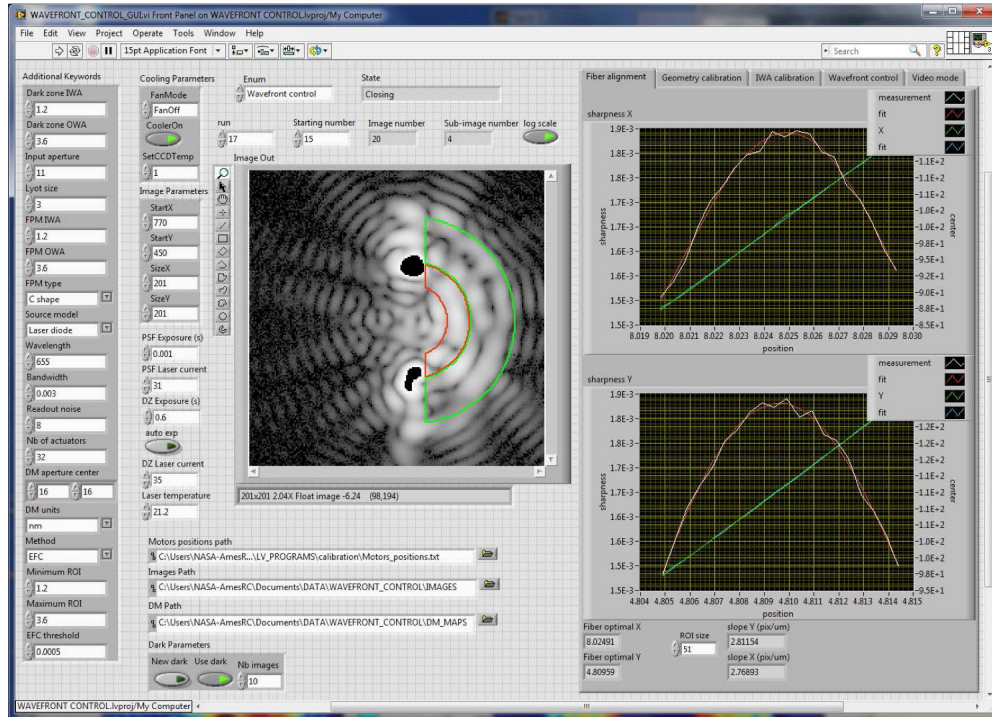

Figure 5. System calibration GUI showing fiber alignment windows. Top right: results from x-motion; Bottom right: results from y-motion. X-axis on both plots represents fiber displacement in mm. Green curve: centroid measurements in pixels (right Y-scale); blue curve: best linear fit to the green curve; white curve: measurement of sharpness (left Y-scale); red: best quadratic fit to sharpness.

2 - Geometric/Metrology and Intensity Calibration

Both the SN and EFC wavefront control algorithms must include high-fidelity knowledge of the optical system geometry to function efficaciously. The DM modulation method (Section 3.4.A, method 1) used to estimate the x-y image scale at the detector focal plane is also used to recalibrate the scale for every run as well as: (a) the rotation between the DM actuator matrix and the array of camera pixels (~ 0.7°); (b) the exact center of the PSF; (c) peak intensity of the resulting speckles.

---

[7] Here we define "sharpness" as $\sum$ image^2 / ($\sum$ image) ^{2} over all pixels in a fixed size photometric aperture capturing all of the (afocal) flux in the PSF core.

3 - *Positioning the Focal Plane Occulting Mask*

The focal plane occulting mask used for the Milestone #1 demonstration was slightly oversized for the 1.2 λ/D milestone IWA requirement; see section 4.1. Thus, the 1.6 λ/D mask had to be offset by 0.4 λ/D to satisfy the geometry of the milestone requirement. To do so the following mask-offset alignment procedure was used:

(1) calculate the total energy of the unocculted on-axis PSF.
(2) move the fiber off-axis to $1.2 * F_L * λ/D$,
        where F_L = focal length of PIAA M1 (900 mm)
           D = clear aperture at the plane of PIAA M1 (87.77 mm)
           λ = 655 nm wavelength of the laser used for the milestone #1 demonstration
(3) incrementally move the mask in one direction (vertical in the test bed layout) and position the mask to have the *maximum* flux occulted.
(4) Incrementally move the mask in the orthogonal direction (horizontally in the test bed layout) to the desired IWA (1.2 λ/D) by finding the position at which the total energy at the detector focal plane is equal to half the total energy in the unocculted PSF.

Figure 6 shows a result of the incremental imaging with the mask motions in steps 3 and 4. In addition to initially positioning the focal plane occulting mask, the stability of the alignment can be rechecked with each wavefront control run to verify that the algorithm has not moved the PSF position behind the mask. The IWA given for the data in this report are from the verification routine.
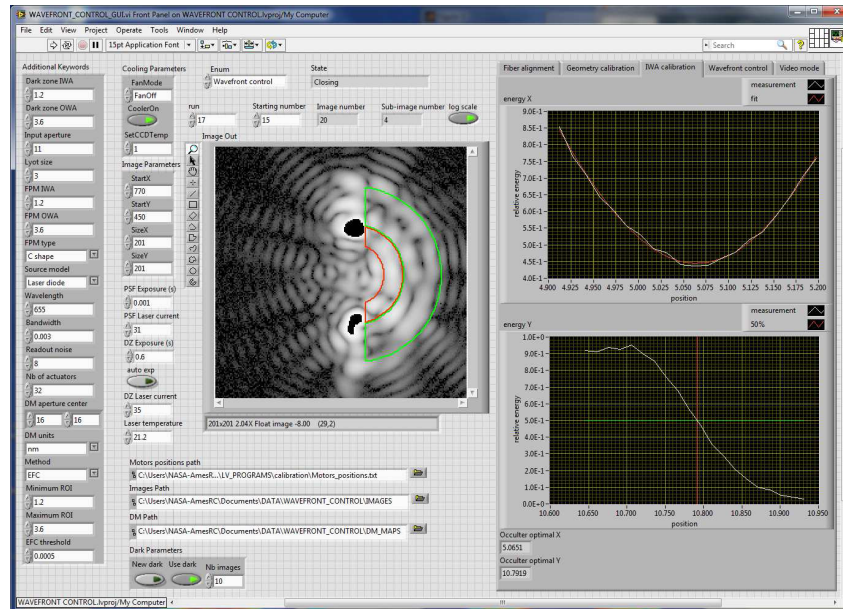

Figure 6: *GUI for the calibration of the inner working angle.*

4 - *Low Order Wavefront Sensor Calibration*

The alignment of the LOWFS was done at the beginning of the whole experiment (manual optical alignment). The LOWFS is then calibrated at the beginning of the run by injecting a

controlled mode (tip and tilt, but in general higher order ones as well) and empirically measuring the differential response of the LOWFS camera to that mode. These responses form a basis of "reference modes" on which future disturbances are decomposed. For more detail, see [23].

4. Milestone #1 Results

4.1. Milestone Procedure

While both EFC and SN were used in the build-up of the test bed procedures to demonstrate system performance to satisfy Milestone #1, ultimately SN was primarily used to satisfy the milestone requirements. Herein we discuss how both were used symbiotically. With either WF control algorithm, the LOWFS control loop was used concurrently executing at all times during each of the test runs.

The mask used for this demonstration (available from the ACE lab without additional procurement costs) was well suited for this demonstration experiment, but was slightly oversized at 1.6 λ/D. Therefore, in order to create a 1.2 λ/D IWA occulted region, the mask was intentionally decentered[8], placing the edge of the mask at 1.2 λ/D. In detail, the wavefront control loop was started with the oversized mask edge at < 1.2 λ/D and then run with incremental repositioning of the mask to increasingly larger IWAs approaching a final 1.2 λ/D configuration for subsequent testing. The combination of SN and LOWFS closed-loop control, with the PIAA coronagraph, allowed us to reach, repeatedly, a median raw contrast of $\leq 10^{-6}$ in the inner (1.2 − 2 λ/D) and < 10^{-7} in the outer (2.0 − 4.0 λ/D) regions as illustrated schematically in Figure 7.
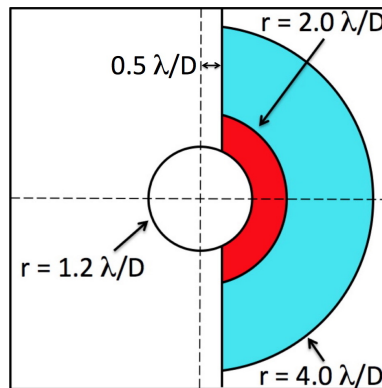
Figure 7: Inner (red) and outer (blue) annular sectors conforming to, and used to verify, Milestone #1 performance.

To measure the electric field, with the EFC algorithm, by phase diversity, EFC modulates the surface of the MEMS DM (changes its shape with a prescribed pattern known as a "probe").

---

[8] The incremental alignment (decentering) of the focal plane occulter was not done closed-loop with the WF control algorithm running. The mask was initially positioned at ~ 1 λ/D and measurements made at that location. With each incremental move toward 1.2 λ/D the WF control algorithm was stopped, and then restarted. This was an initial configuration procedure only.

With EFC, the (manually) selectable control loop gain is high when (initially) the contrast is low, and declines to zero (with the probes then turned off) as the milestone goal is reached and/or exceeded. With zero gain, EFC is reduced to a simple sequence of CCD images at the identical (static) MEMS DM settings. We found our test bed system was quite stable throughout the measurement periods after initially resetting the DM. Thus, in the stability (repeatability) graphs presented in Fig 11, our EFC loop was simply a sequence of 1500 science camera images contiguously acquired with "probes off" for a little over one hour. However, incoherent light (arising from image ghosts, instrumental scattering, polarization, etc.) cannot be measured, so we also ran EFC for 50 images with "probes on" to get a good sampling of the incoherent light. So, basically, the process after mask alignment and DM reset is summarized as:

(1) Use SN to achieve high contrast.
(2) Then take 1500 images without any WF control algorithm actively running[9].
(3) Use EFC to measure the coherent light, enabling the calculation of the incoherent light as follows:
  (a) Measure the electric field in the image plane using EFC (giving the amount of coherent light).
  (b) Get the electric field intensity, I_{est}, estimated from EFC
  (c) Subtract I_{est} from the actual measured intensity from the science camera image
(3c) thus gives the incoherent light in the image.
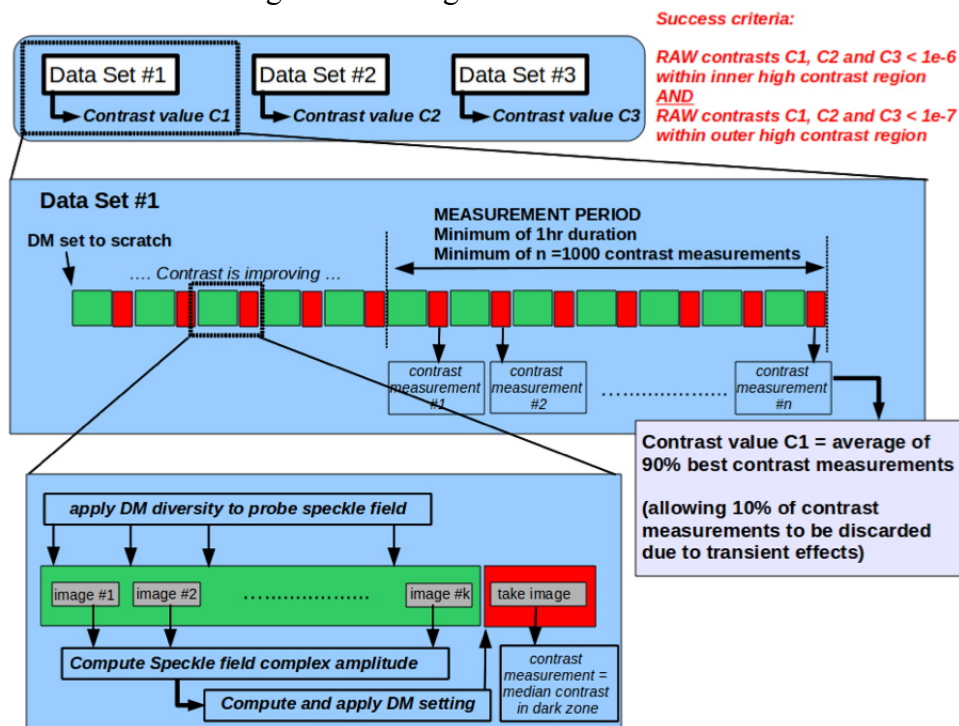
Figure 8: Definition of the milestone data acquisition sequence.

Instantaneous measurements of the coronagraphic contrast field, per section 4.4 of JPL Document D-75787, were derived from data acquired with the science camera, with the

---

[9] This was possible because of the stability of the system over the "run" timescale of approximately one hour. This is technically equivalent to taking images with either EFC or SN and the loop gain set to zero.

wavefront control system active, in trial "runs" of 1500 contiguous measurements after resetting the DM following the Milestone #1 demonstration procedure as prescribed in section 4.6 (steps 4.6.1 – 4.6.5) of JPL Document D-75787. We reproduce from that section, here in Figure 8, a schematic representation of the image acquisition timeline. "Data sets" resulting from each trial run, as defined in step 4.5.6 of the aforementioned procedure were produced and archived from these raw and calibrated data. After initial experiments with the hardware and wavefront control software, after approximately 60 trial runs the system was reproducible meeting the milestone #1 contrast requirements.

4.2. Certification Data Package and Summary

Per section 5 of JPL Document D-75787, and in particular item 5.4 to provide evidence of the repeatability of the contrast demonstration, an electronically downloadable[10] Certification Data Package has been prepared and is available to the NASA Exoplanet Exploration Office for independent review and analysis.

In Figure 9, we summarize and present the principal results of the investigation, demonstrating repeatable milestone #1 IWA/raw contrast performance, from three typically representative trial runs[11]. The originating data sets, inclusive of calibration data files, are available for inspection and/or independent analysis/verification in the Certification Data Package (CDP) and are identified with each of the sets of the reduced images and graphics illustrated.

For each of the three illustrative runs in Figure 9, we present (dark subtracted) image contrast maps, (intra-run) stability time series of median contrasts in the two control zones, and estimates of the median incoherent light[12] in the two control zones. The image raw contrast maps are (arbitrarily) for the last (1500th) image in each run using SN. The incoherent light maps are computed as per step (3b) as in section 4.1, using EFC.

---

[10] Access information to a UofA server hosting the CDP for electronic download via sftp separately provided to the NASA EXEP office.

[11] The Matlab code that was used to create these figures is called batch_milestone_Set1.m and is available in the CDP.

[12] We believe that most of the incoherent light detected is due to model errors, as we do not have the exact distances and the exact phase maps of all the optics in the system.
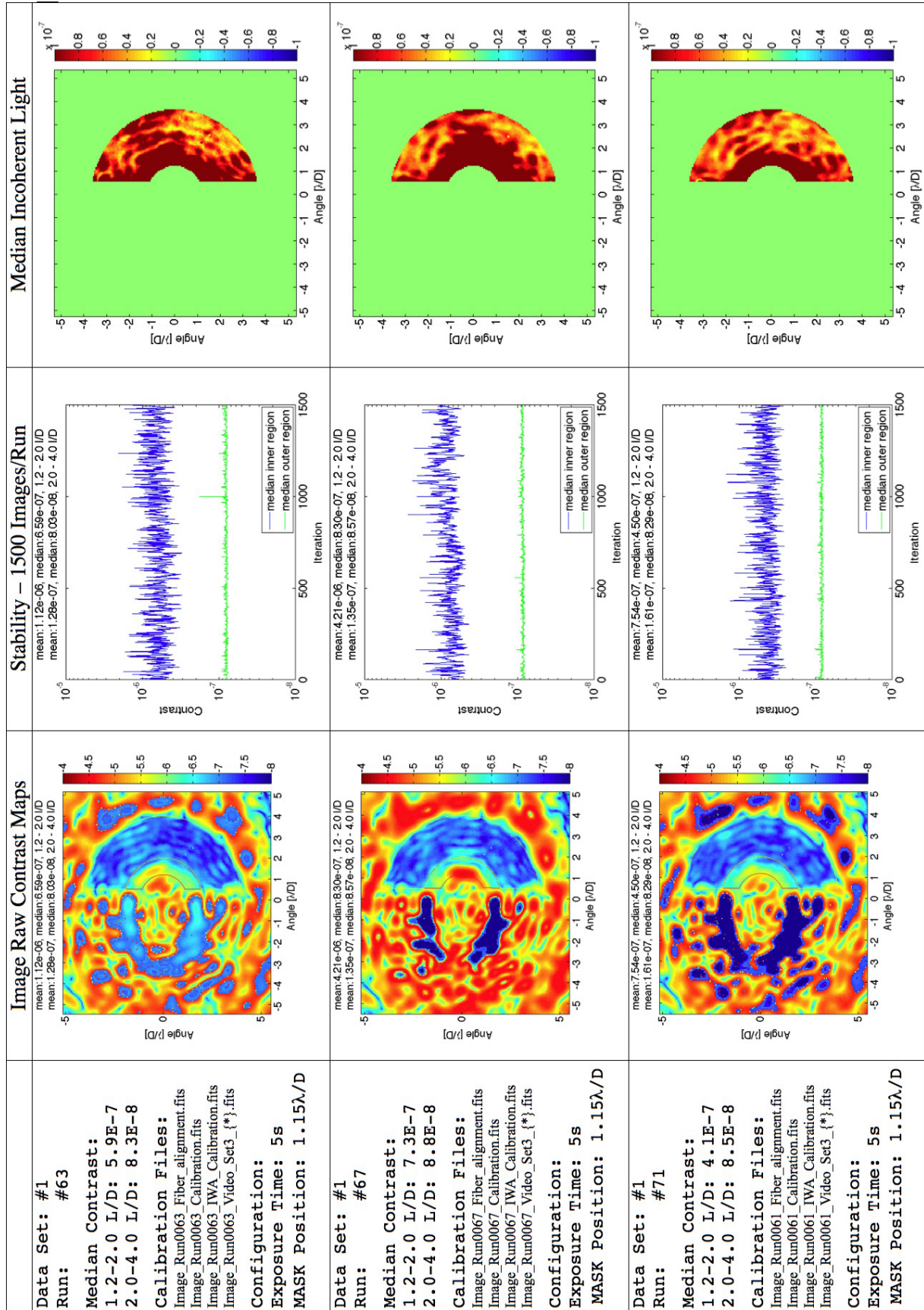
Image Raw Contrast Maps

Data Set: #1
Run: #63

Median Contrast:
1.2-2.0 L/D: 5.9E-7
2.0-4.0 L/D: 8.3E-8

Calibration Files:
Image_Run0063_Fiber_alignment.fits
Image_Run0063_Calibration.fits
Image_Run0063_IWA_Calibration.fits
Image_Run0063_Video_Set3_{*}.fits

Configuration:
Exposure Time: 5s
MASK Position: 1.15λ/D

mean:1.12e-06, median:6.59e-07, 1.2 - 2.0 l/D
mean:1.28e-07, median:8.03e-08, 2.0 - 4.0 l/D

Data Set: #1
Run: #67

Median Contrast:
1.2-2.0 L/D: 7.3E-7
2.0-4.0 L/D: 8.8E-8

Calibration Files:
Image_Run0067_Fiber_alignment.fits
Image_Run0067_Calibration.fits
Image_Run0067_IWA_Calibration.fits
Image_Run0067_Video_Set3_{*}.fits

Configuration:
Exposure Time: 5s
MASK Position: 1.15λ/D

mean:4.21e-06, median:8.30e-07, 1.2 - 2.0 l/D
mean:1.35e-07, median:8.57e-08, 2.0 - 4.0 l/D

Data Set: #1
Run: #71

Median Contrast:
1.2-2.0 L/D: 4.1E-7
2.0-4.0 L/D: 8.5E-8

Calibration Files:
Image_Run0061_Fiber_alignment.fits
Image_Run0061_Calibration.fits
Image_Run0061_IWA_Calibration.fits
Image_Run0061_Video_Set3_{*}.fits

Configuration:
Exposure Time: 5s
MASK Position: 1.15λ/D

mean:7.54e-07, median:4.50e-07, 1.2 - 2.0 l/D
mean:1.61e-07, median:8.29e-08, 2.0 - 4.0 l/D

Stability – 1500 Images/Run

Median Incoherent Light

Figure 9 – Visualization milestone #1 demonstration – results meeting requirements and reproducibility

5. References

[1] Guyon, O., Schneider, G., Belikov, R., Tenerelli, D., 2012, "The EXoplanetary Circumstellar Environments and Disk Explorer (EXCEDE)", in Society of Photo-Optical Instrumentation Engineers (SPIE) Conference Series, 8442, 1

[2] Guyon, O., 2003, "Phase-induced amplitude apodization of telescope pupils for extrasolar terrestrial planet imaging", A&A, 404, 379

[3] Traub, Wesley A.; Vanderbei, Robert J., 2003, "Two-Mirror Apodization for High-Contrast Imaging", ApJ, 599, 695

[4] Vanderbei, Robert J., Traub, Wesley A., 2005, "Pupil Mapping in Two Dimensions for High-Contrast Imaging", ApJ, 626, 1079

[5] Guyon, O., Pluzhnik, E.A., Galicher, R., Martinache, F., Ridgway, S.T., Woodruff, R.A., 2005, "Exoplanet Imaging with a Phase-induced Amplitude Apodization Coronagraph. I. Principle", ApJ, 622, 744

[6] Martinache, F., Guyon, O., Pluzhnik, E.A., Galicher, R., Ridgway, S. T., 2006, "Exoplanet Imaging with a Phase-Induced Amplitude Apodization Coronagraph. II. Performance", ApJ, 639, 1129

[7] Vanderbei, R. J., 2006, "Diffraction Analysis of Two-dimensional Pupil Mapping for High-Contrast Imaging", ApJ, 636, 528

[8] Pluzhnik, E. A., Guyon, O., Ridgway, S. T., Martinache, F., Woodruff, R. A., Blain, C., Galicher, R., 2006, "Exoplanet Imaging with a Phase-Induced Amplitude Apodization Coronagraph. III. Diffraction Effects and Coronagraph Design", ApJ, 644, 1246

[9] Guyon, O., Pluzhnik, E.A., Kuchner, M. J., Collins, B., Ridgway, S.T., 2006, "Theoretical Limits on Extrasolar Terrestrial Planet Detection with Coronagraphs", ApJ Suppl, 167, 81

[10] Lozi, J., Martinache, F., Guyon, O., 2009, "Phase-Induced Amplitude Apodization on centrally obscured pupils: design and first laboratory demonstration for the Subaru Telescope pupil", PASP, 121, 1232

[11] Guyon, O., Martinache, F., Belikov, R., Soummer, R., 2010, "High Performance PIAA Coronagraphy with Complex Amplitude Focal Plane Masks", ApJ Suppl, 190, 220

[12] Guyon, O., Pluzhnik, E. A., Martinache, F., Totems, J., Tanaka, S.; Matsuo, T.; Blain, C., Belikov, R., 2010, "High Contrast Imaging and Wavefront Control with a PIAA Coronagraph: Laboratory System Validation", PASP, 122, 71

[13] Guyon, O., Matsuo, T., Angel, R., 2009, "Coronagraphic Low Order Wavefront Sensor: Principle and Application to a Phase-Induced Amplitude Coronagraph", ApJ, 693, 75-

[14] Belikov, R., Pluzhnik, E., Witteborn, F. C., Greene, T. P., Lynch, D.H., Zell, P. T., Guyon, O., 2011, "Laboratory demonstration of high-contrast imaging at inner working angles 2 λ/D and better", Proc SPIE, 8151, 1

[15] Phase-induced amplitude apodization M1 mirror re-figuring, http://prod.nais.nasa.gov/cgi-bin/eps/synopsis.cgi?acqid=136681

[16] Levine, M. et al., 2009, "Terrestrial Planet Finder – Coronagraph (TPF-C) Flight Baseline Mission Concept", white paper provided to the 2010 Decadal Survey

[17] Give'on, A., Kern, B., Shaklan, S., Moody, D. C., Pueyo, L., 2007, "Broadband wavefront correction algorithm for high-contrast imaging systems", Proc. SPIE, 6691, 7

[18] Bordé P. J., Traub W. A., 2006, "High-Contrast Imaging from Space: Speckle Nulling in a Low-Aberrations Regime", ApJ 638, 488

[19] Savransky, D., Macintosh, B. A., Thomas, S. J., Poyneer, L. A., Palmer, D. W. , De Rosa, R. J. and Har-tung M., 2012, "Focal plane wavefront sensing and control for ground-based imaging," in Society of Photo-Optical Instrumentation Engineers (SPIE) Conference Series, 8447, 6

[20] Hinkley, S., Oppenheimer, B. R., Brenner, D., Parry, I. R., Sivaramakrishnan, A., Soummer, R. and King, D., 2008, "A new integral field spectrograph for exoplanetary science at Palomar," in ," in Society of Photo-Optical Instrumentation Engineers (SPIE) Conference Series 7015, 32

[21] Guyon, O., Martinache, F., Garrel, V., Vogt, F., Yokochi, K., and Yoshikawa, T., 2010, "The Subaru coronagraphic extreme AO (SCExAO) system: wavefront control and detection of exoplanets with coherent light modulation in the focal plane," in Society of Photo-Optical Instrumentation Engineers (SPIE) Conference Series 7736, 71

[22] Martinache, F., Guyon, O., Clergeon, C., and Blain, C., 2012, "Speckle Control with a Remapped-Pupil PIAA Coronagraph," PASP, 124, 1288

[23] Lozi, J., Belikov, R., Schneider, G., Guyon, O., Pluzhnik, E., Thomas, S. J., Martinache F., "Experimental Study of a Low-Order Wavefront Sensor for the High-Contrast Coronagraphic Imager EXCEDE", 2013, in Society of Photo-Optical Instrumentation Engineers (SPIE) Conference Series, 8864, 23

6. ACRONYM LIST

ACE	(NASA) Ames Coronagraph Experiment
ARC	(NASA) Ames Research Center
CCD	Charged Coupled Device
CDP	Certification Data Package
DM	Deformable Mirror
EFC	Electric Field Conjugation
EXCEDE	Exoplanetary Circumstellar Environments and Disk Explorer
GUI	Graphical User Interface
IWA	Inner Working Angle
JPL	Jet Propulsion Laboratory
LOWFS	Low Order Wave-Front Sensor
MEMS	Micro Electro Mechanical System
PI	Principal Investigator
PIAA	Phase Induced Amplitude Apodization
PSF	Point Spread Function
SN	Speckle Nulling
TM&D	Technology Maturation & Demonstration
UofA	University of Arizona